JOURNAL OF NEUROTRAUMA 33:662–671 (April 1, 2016)

DOI: 10.1089/neu.2015.4002

Manganese-Enhanced Magnetic Resonance Imaging as a Diagnostic and Dispositional Tool after Mild-Moderate Blast Traumatic Brain Injury

Olga Rodriguez,[1] Michele L. Schaefer,[2] Brock Wester,[3] Yi-Chien Lee,[4] Nathan Boggs,[3] Howard A. Conner,[3] Andrew C. Merkle,[3] Stanley T. Fricke,[5] Chris Albanese,[4,6,*] and Vassilis E. Koliatsos[7,8,*]

Abstract

Traumatic brain injury (TBI) caused by explosive munitions, known as blast TBI, is the signature injury in recent military conflicts in Iraq and Afghanistan. Diagnostic evaluation of TBI, including blast TBI, is based on clinical history, symptoms, and neuropsychological testing, all of which can result in misdiagnosis or underdiagnosis of this condition, particularly in the case of TBI of mild-to-moderate severity. Prognosis is currently determined by TBI severity, recurrence, and type of pathology, and also may be influenced by promptness of clinical intervention when more effective treatments become available. An important task is prevention of repetitive TBI, particularly when the patient is still symptomatic. For these reasons, the establishment of quantitative biological markers can serve to improve diagnosis and preventative or therapeutic management. In this study, we used a shock-tube model of blast TBI to determine whether manganese-enhanced magnetic resonance imaging (MEMRI) can serve as a tool to accurately and quantitatively diagnose mild-to-moderate blast TBI. Mice were subjected to a 30 psig blast and administered a single dose of $MnCl_2$ intraperitoneally. Longitudinal T1-magnetic resonance imaging (MRI) performed at 6, 24, 48, and 72 h and at 14 and 28 days revealed a marked signal enhancement in the brain of mice exposed to blast, compared with sham controls, at nearly all time-points. Interestingly, when mice were protected with a polycarbonate body shield during blast exposure, the marked increase in contrast was prevented. We conclude that manganese uptake can serve as a quantitative biomarker for TBI and that MEMRI is a minimally-invasive quantitative approach that can aid in the accurate diagnosis and management of blast TBI. In addition, the prevention of the increased uptake of manganese by body protection strongly suggests that the exposure of an individual to blast risk could benefit from the design of improved body armor.

Key words: blast-induced neurotrauma; blast injury; manganese-enhanced MRI (MEMRI); traumatic brain injury

Introduction

Traumatic brain injury (TBI) from explosive munitions, also known as blast TBI, is the signature injury in the Iraq and Afghanistan war theaters.[1,2] Most cases of blast TBI are mild in severity and present with clinical symptoms indistinguishable from those of blunt concussion. Blast TBI often occurs in a repetitive pattern, and this pattern may be the cause of chronic neuropsychiatric conditions in veterans of these conflicts, just as in the case of athletes with histories of repeat concussions from contact and collision sports. In some cases, such repetitive TBI exposure may lead to chronic traumatic encephalopathy, a degenerative tauopathy.[3,4] Prevention of chronic symptomatologies and neurodegenerative disease after concussion is based on the avoidance of repeat exposure to TBI-producing events until patients become asymptomatic. This principle is at the root of several versions of return-to-play or combat guidelines issued by international conferences, clinical professional associations, the Centers for Disease Control and Prevention, and the U.S. military (www.dvbic.org). Although such guidelines are based on established clinical practice

[1]Department of Oncology, Lombardi Comprehensive Cancer Center, Georgetown University Medical Center, Washington, DC.
[2]Department of Anesthesiology and Critical Care Medicine, [7]Department of Pathology, [8]Department of Neurology, Johns Hopkins University School of Medicine, Baltimore, Maryland.
[3]Research and Exploratory Development Department, Johns Hopkins University, Applied Physics Laboratory, Laurel, Maryland.
[4]Department of Oncology, [6]Department of Pathology, Georgetown University Medical Center, Washington DC.
[5]Pediatric and Integrative Systems Biology, George Washington University, Washington, DC.
*These authors contributed equally.

and are generally designed to be on the ''safe side'' of decision-making, it is impossible to predict, for each individual soldier or athlete, the long-term outcome of re-exposure to TBI.

It has been argued that the best way to base decisions regarding redeployment or return-to-play is to follow relevant quantifiable post-TBI changes based on brain imaging or non-imaging biomarkers.[5–8] Such markers could help determine at which point re-exposure to TBI risk is acceptable. Further, because of the acute and chronic neuropathological consequences of TBI, early detection also may assist in prompt and thus more effective interventions.

Magnetic resonance imaging (MRI) is a particularly appealing imaging modality because it is non-invasive and causes only minimal distress to the patient. Unfortunately, blast TBI, especially of the more common mild variety, is not easy to diagnose with structural imaging because it is neither associated with marked morphometric or pathological changes, such as overt edema, bleeding, midline shift, or atrophy, nor does it generate sufficient imaging contrast when using blood pool contrast agents currently available in the clinic.

The divalent manganese ion (Mn^{2+}) is a paramagnetic compound that was recognized as the first MRI T1 contrast agent several decades ago. In fact, the use of Mn^{2+} as a contrast agent parallels the history of the application of nuclear magnetic resonance (NMR) in biological studies.[9–14] The use of $Mn2^{+}$ as a contrast agent in MRI, termed manganese-enhanced MRI (MEMRI), was pioneered in studies of neural activity, tract-tracing, and neuroarchitecture by Koretsky and colleagues in the 1990s.[10,15–18] When administered orally or parenterally, Mn^{2+} accumulates in all body tissues and is excreted via the biliary system,[19–21] a condition that explains its use, in a chelated form, to assess liver and pancreatic pathologies in Europe.[19,22–24] After systemic injection, Mn^{2+} enters the brain promptly through the cerebrospinal fluid (CSF), thereby first reaching the ventricles, choroid plexus, and regions that lack a blood–brain barrier (BBB), such as the pituitary and pineal glands and the median eminence. After crossing the BBB, Mn^{2+} can be incorporated into brain cells via active transport through calcium-channels and other metal transporters[25–29] and it can persist inside cells for weeks or months.[30–32] The usefulness of MEMRI in visualizing the effects of trauma on brain structures was first demonstrated in a mouse model of diffuse TBI.[33]

In the present study, we explored changes in the MEMRI signal using a mouse model of mild-to-moderate blast exposure. We found that mice exposed to blast showed a rapid and significant increase in brain Mn^{2+} uptake. In addition, we found that such an increase was prevented by shielding of the torso, a strategy previously shown by us to protect the brain from the neuropathological consequences of blast.[34,35] Our findings indicate that MEMRI may serve as a non-invasive tool for the rapid and accurate diagnosis of blast TBI.

Methods

Experimental subjects and blast exposure

Mice (C57BL6/J, male; Jackson Laboratories, Bar Harbor, ME) were anesthetized with 4% isoflurane in a gas mixture of 30% oxygen and 70% nitrous oxide, fixed on a wire-mesh holder, and positioned at the open end of the shock tube facing the shockwave front. Our blast model was designed to minimize head movement and thus prevent, to the extent possible, acceleration/deceleration injury. Toward this goal, the head was tethered on the mesh through the frontal teeth. Anesthetized animals were exposed to a single mild-moderate blast event (corresponding to 30 psig of membrane rupture pressure) in the supine position in a helium-driven shock tube as previously described.[35,36] Animals were divided into three groups that were exposed to 1) whole–body blast ($n=12$); 2) blast with a polycarbonate jacket for torso protection with chest, abdomen, and limbs covered ($n=5$) as described previously[35,36]; and 3) no blast exposure (sham; $n=10$). Fifteen minutes after exposure, animals were injected intra-peritoneally with a single dose of 40 mg/kg of $MnCl_2$ and subcutaneously with 200 μL of neutral phosphate-buffered saline.[37] The $MnCl_2$ solution was prepared as described previously.[37] Briefly, 100 mM of highly purified $MnCl_2 \cdot 4H20$ (product number 529680; Sigma-Aldrich) were dissolved in 100 mM bicine solution and adjusted to pH 7.4. Control mice were not exposed to blast nor did they receive $MnCl_2$. All procedures involving animals were approved by the Animal Care and Use Committees of Johns Hopkins and Georgetown Universities.

MRI

MRI was performed in a 7-Tesla horizontal Bruker spectrometer run by Paravision 5.1 as previously described.[38–44] Animals were imaged after a 6-h recovery post-blast. Anesthetized mice (1.5% isoflurane in a gas mixture of 30% oxygen and 70% nitrous oxide) were placed on our in-house designed and custom-manufactured stereotaxic device (ASI Instruments, Warren, MI) with built-in temperature and cardio-respiratory monitoring engineered to fit a Bruker 4-channel phased-array mouse brain coil and a corresponding transmit volume coil. T2-weighted rapid acquisition with relaxation enhancement (RARE) sequences were used to identify key neuropathologies such as bleeding, hematomas, edema, or gross changes in brain structure. T1-weighted sequences were then used to visualize changes in contrast related to $MnCl_2$ uptake. The MEMRI imaging protocol was a T1-weighted two-dimensional RARE sequence with the following parameters: repetition time (TR), 1650 msec; echo time (TE), 10.6 msec; inversion time (TI), 650 msec; field of view (FOV), 3.0 cm; RARE factor, 2; matrix, 256×256; averages, 1; slice thickness, 1 mm. A custom-designed 0.01 mM $MnCl_2$ phantom was positioned inside the brain coil above the animal head and used as an internal standard.

The MRI protocol used for gadolinium experiments was a T1-weighted RARE sequence with the following parameters: TR, 300 msec; TE, 10.2 msec; FOV, 3.0 cm; RARE factor, 1; matrix, 256×256; averages, 4; slice thickness, 0.75 mm.

Image analysis

Image processing, normalization, and quantification were performed with Paravision 5.1 Processing Software (Bruker, Billerica, MA). Regions of interest (ROIs) located on different areas of the brain and on the $MnCl_2$ phantom were selected from the MR images, and the mean contrast in the gray scale was measured at 6, 24, 48, and 72 h and at 14 and 28 days after blast. (Fig. 1). ROIs were of the same size and shape in all subjects. Image contrast data for each ROI were normalized to contrast data in the $MnCl_2$ phantom.

Statistical analysis

Data were analyzed by one-way analysis of variance (ANOVA). Mean intensities in the gray scale were measured for each brain ROI at the time-points mentioned above. Table 1 shows the ANOVA data with p values for every region and every time-point.

Results

Anatomical and contrast-enhanced imaging

T2-weighted MRI was first performed to rule out the presence of hematoma, hemorrhage, or edema; these conditions can dramatically increase the uptake of Mn^{2+} due to the disruption of the BBB

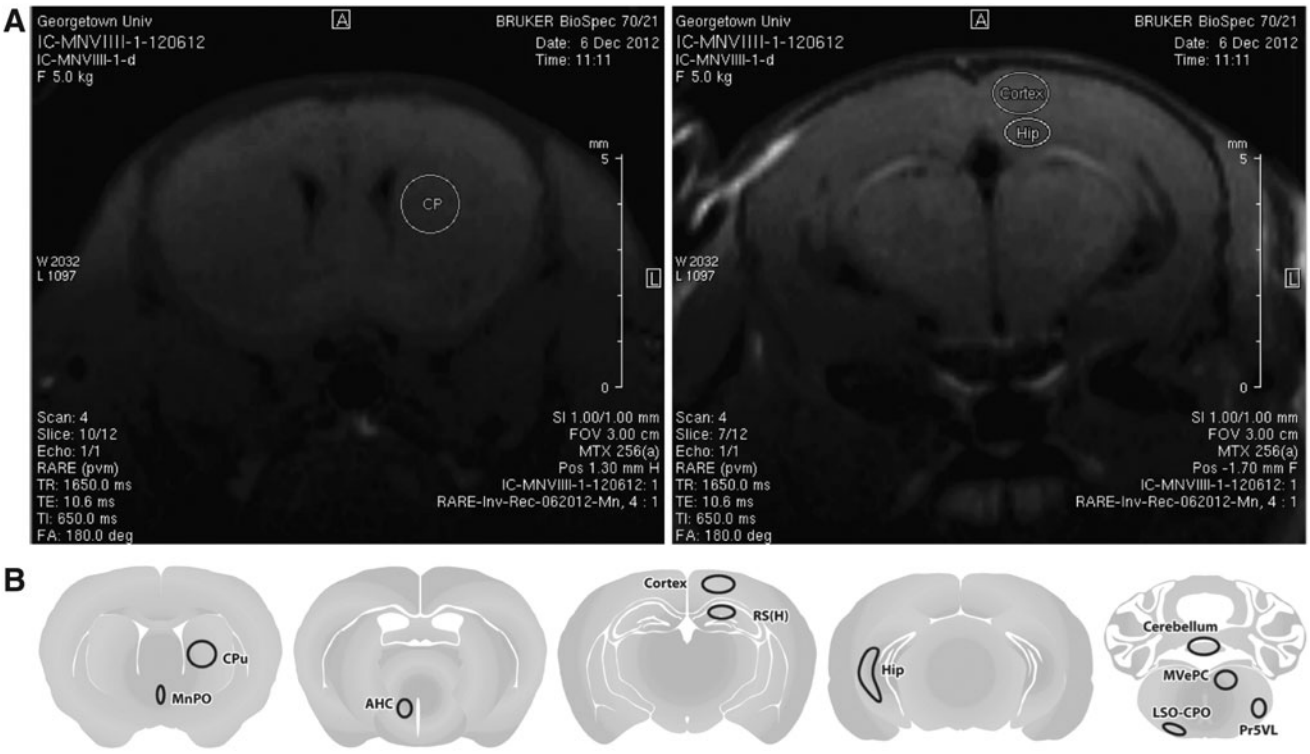

FIG. 1. Regions of interest (ROIs) were selected in a number of brain areas on the anatomical T1-weighted rapid acquisition with relaxation enhancement (RARE) images **(A)** acquired after exposure to blast and the administration of the $MnCl_2$ contrast agent. The mean intensity in the gray scale was determined for every ROI at 6, 24, 48, 72 h, and 14 and 28 days after injury. A schematic representation of all ROIs **(B)** are depicted for caudate putamen, median preoptic nucleus, anterior nucleus hypothalamus, cortex, hippocampus-CA1/CA3/DG, hippocampus-CA1, cerebellum, medial vestibular nucleus, lateral superior olivary nucleus, and principal sensory trigeminal nucleus.

and thus produce confounding results. No such pathologies were detected in any of our experimental subjects (data not shown). Next, T1-weighted MEMRI was performed as described in the Methods section. Mice with blast TBI showed a marked increase in positive contrast, compared with sham controls (Fig. 2).

In particular, at 6 h post-blast, there was a marked signal increase in the choroid plexus of the interventricular region (tela choroidea) and in associated periventricular structures, such as the fornix and the neostriatum, a distribution pattern that reflects the diffusion of Mn^{2+} across the blood–CSF barrier, as described previously.[31,32] Sham controls that had not been exposed to blast but received the $MnCl_2$ injection did not exhibit this change (Fig. 2, left panel). Twenty-four hours after blast, T1-weighted MEMRI showed that the signal increase had shifted from ventricular to periventricular regions and was homogenously dispersed throughout the brain with a marked accentuation of anatomical structures (Fig. 2, right panel). Once again, sham control subjects showed a significantly lower enhancement at the dose of $MnCl_2$ used. This phenomenon is better visualized after pseudo-color processing of the images (Fig. 3).

The single dose of $MnCl_2$ dose used in our study (40 mg/kg) had little effect on mortality and morbidity. Only two mice died during the course of the experiment. These deaths occurred in the second week after the injury and, therefore, 2 weeks post-$MnCl_2$ injection. At this time-point, any potential negative effects of $MnCl_2$ are expected to be minimal. For this reason, we suspect that these deaths were unrelated to the contrast agent.

Table 1. Analysis of Variance—*p* Values in Selected Regions of Interest

	6 h	*24 h*	*48 h*	*72 h*	*7 d*	*14 d*	*28 d*
Cortex	0.004	<0.001	<0.001	0.003	<0.001	0.018	0.369
Regio superior hippocampus	0.008	0.001	0.002	0.003	0.002	0.035	0.51
Caudate putamen	0.004	0.001	0.001	0.003	<0.001	0.019	0.182
Median preoptic nucleus	0.003	<0.001	<0.001	0.002	<0.001	0.006	0.1
Cerebellum	0.025	0.003	0.033	0.018	0.015	0.095	0.465
Hypothalamus	0.001	<0.001	0.001	0.002	<0.001	0.009	0.05
Hippocampus	0.004	0.001	0.022	0.012	0.001	0.014	0.438
Olivary–preolivary nucleus	0.032	0.007	0.05	0.031	0.043	0.122	0.643
Sensory trigeminal nucleus	0.071	0.005	0.033	0.052	0.022	0.071	0.67
Medial vestibular nucleus	0.278	0.049	0.18	0.322	0.43	0.538	0.414

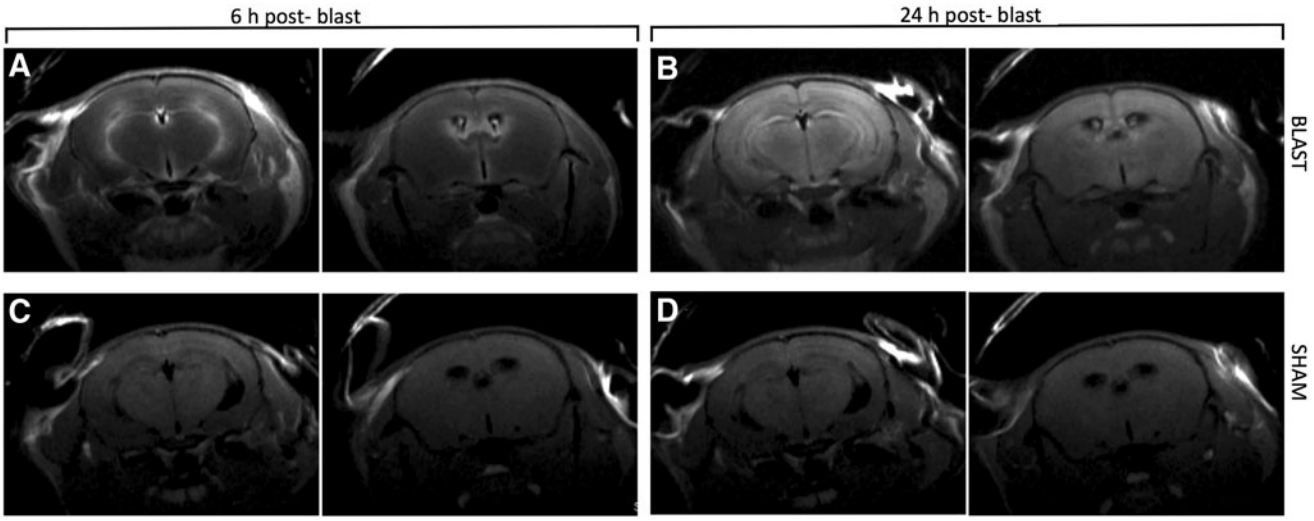

FIG. 2. Six hours after blast and $MnCl_2$ injection, positive contrast is markedly increased in ventricular and periventricular areas **(A)**. Manganese-enhanced magnetic resonance imaging performed 24 h after blast reveals a diffuse pattern of contrast increase throughout the brain parenchyma **(B)**. Uptake of contrast agent is significantly less prominent in sham controls at both time-points **(C, D)**.

Quantitative changes

Post-acquisition image analyses were performed to quantify changes in image contrast. To this effect, several regions of interest (ROIs) were selected on serial T1-weighted MR images and mean intensity values were quantified using Paravision 5.1 (Fig. 4). A $MnCl_2$ phantom was affixed to the brain array coil for normalization as described in the Methods section. Mean intensity values in phantom ROIs demonstrated a greater-than-expected variation over the course of the month-long experiment. This variation was not explained by daily drifts in magnetic frequency, temperature or other factors, and ROIs delineated on the background of the image did not show these variations, a pattern indicating that imaging conditions were consistent over time. We therefore concluded that the variability in the mean intensity values of phantoms was the result of microscopic air bubbles and slight changes in the position of phantoms. For the above reasons, we decided to use instead non-blast exposed mice injected with vehicle ($n=4$) as imaging quality controls. In the absence of $MnCl_2$, these subjects were not expected to show an increase in contrast and could thus be used to establish baseline T1 values. Therefore, specific ROIs in $MnCl_2$-treated blast and $MnCl_2$-treated sham mice were normalized to ROIs localized in comparable regions in sham-vehicle mice.

T1 contrast enhancement was significantly increased in mice exposed to blast, compared with sham mice, in all brain regions examined (Fig. 4). Differences in mean intensity values were significant in all ROI during the first week after blast injury (Table 1). Differences were still present in select regions at 2 weeks but disappeared one month after injury.

Mn^{2+} is known to accumulate in tissues progressively over the course of several days. In our study, the MEMRI T1 signal continued to increase up to 72 h post-blast, after which it progressively diminished until it reached baseline by 1 month. It should be mentioned that mice were not imaged before administration of $MnCl_2$ and therefore the first value depicted in graphs (at 6 h) does not correspond to a true baseline contrast.

To determine whether the rapid and marked uptake of Mn^{2+} was primarily caused by a breakdown of the BBB, we performed contrast-enhanced MRI with the contrast agent gadopentetate

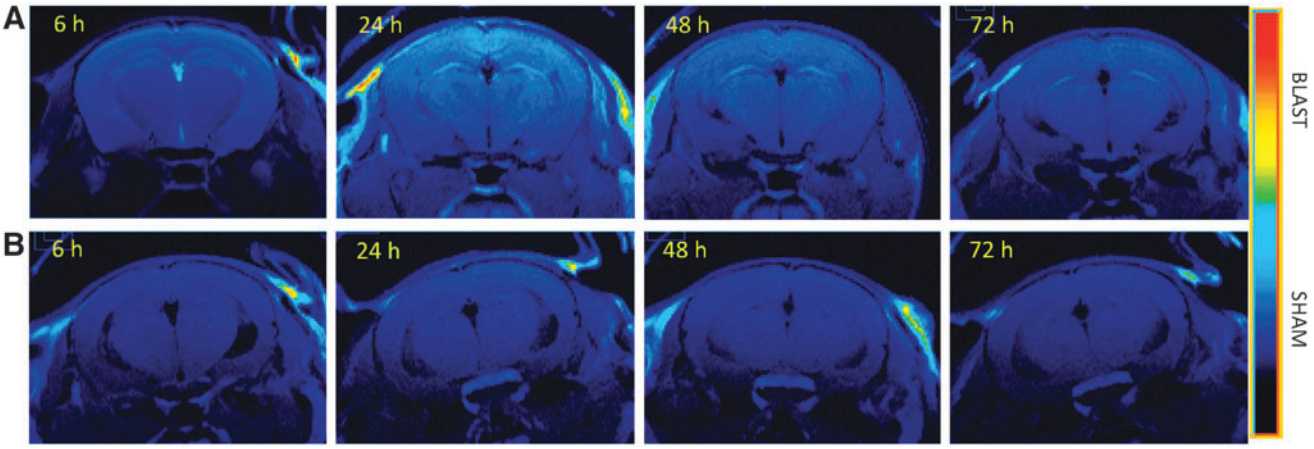

FIG. 3. Pseudo-color processing applied to gray scale images. Image manipulation highlights the difference in contrast between blast-injured **(A)** and sham mice **(B)** after injection of $MnCl_2$.

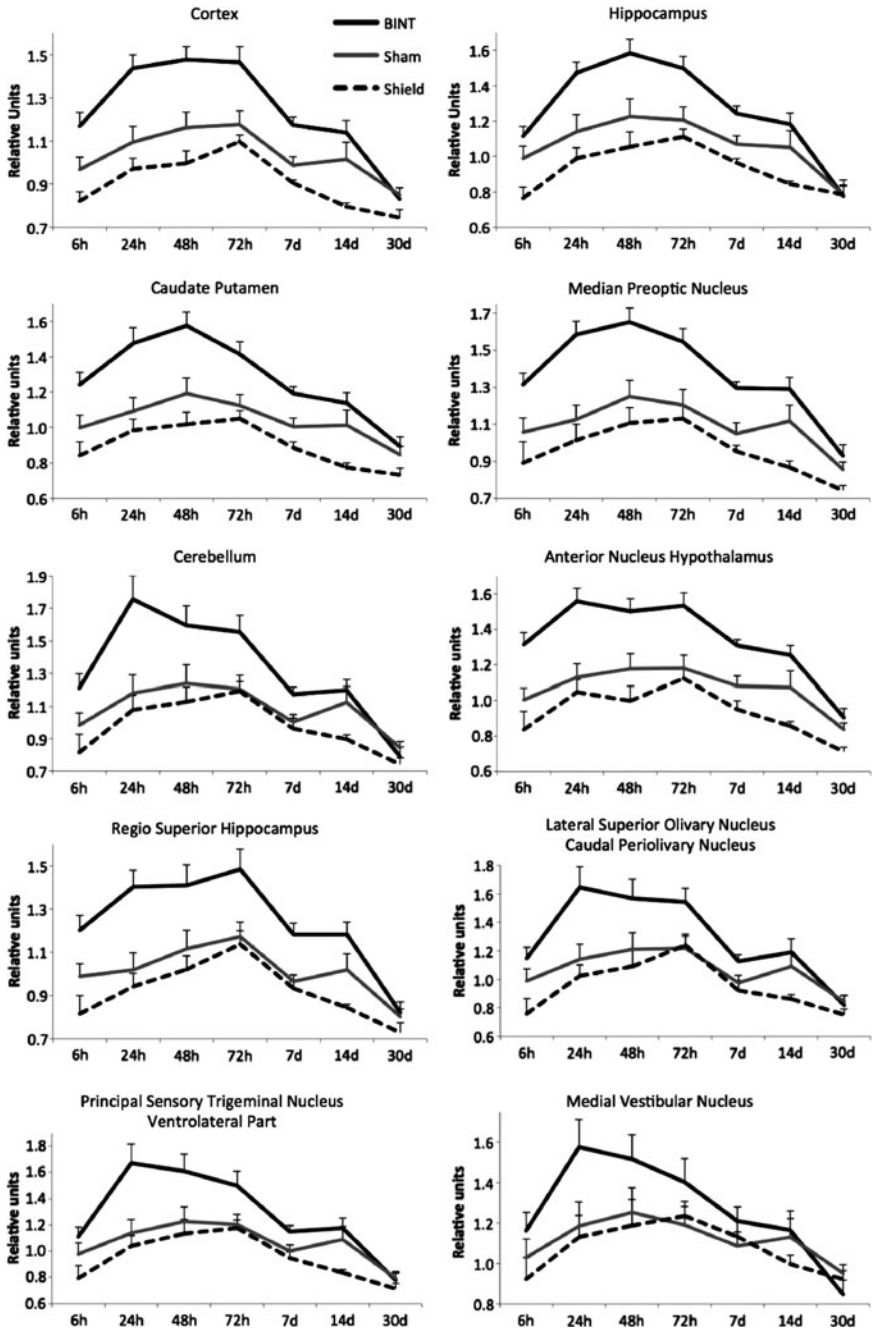

FIG. 4. Mean intensity values in selected brain regions of interest (ROIs) of blast-injured mice with and without polycarbonate torso protection (shield). Mean values were normalized to values in corresponding areas in vehicle-treated mice.

dimeglumine (Gd). MRI with Gd-based contrast agents is the accepted standard for the assessment of the integrity of the blood–brain barrier.[45–50] When the brain vasculature becomes abnormal, Gd leakage causes signal enhancement in the surrounding tissues. A dose of Gd of 0.3 mmol/kg was injected subcutaneously at 6, 24, and 72 h and at 7, 14, and 28 days after blast. MRI was performed 20 min after injection; this time frame was chosen based on previous DCE-MRI experiments we performed on C57/Bl6 mice with brain tumors and penetrating TBI in which we determined that Gd contrast in mice with BBB disruption reached a maximum 15 min after bolus injection and remained constant for approximately 1.5 h. Blast-injured mice did not show contrast enhancement in any of the brain ROI selected but did exhibit hyperintensity in midline vascular structures and a lateral ventricular entity that is likely the choroid plexus (Fig. 5). On the other hand, an ROI placed on neck muscle showed a 35% increase in positive contrast. This result indicates that the excessive influx of Mn^{2+} into the brain after blast exposure is not simply due to vascular pathology and extravasation.

Effects of systemic protection on imaging findings

Based on our previous findings showing that torso and upper abdomen protection prevents neuropathological and behavioral changes after blast exposure,[35] we explored whether body protection with a

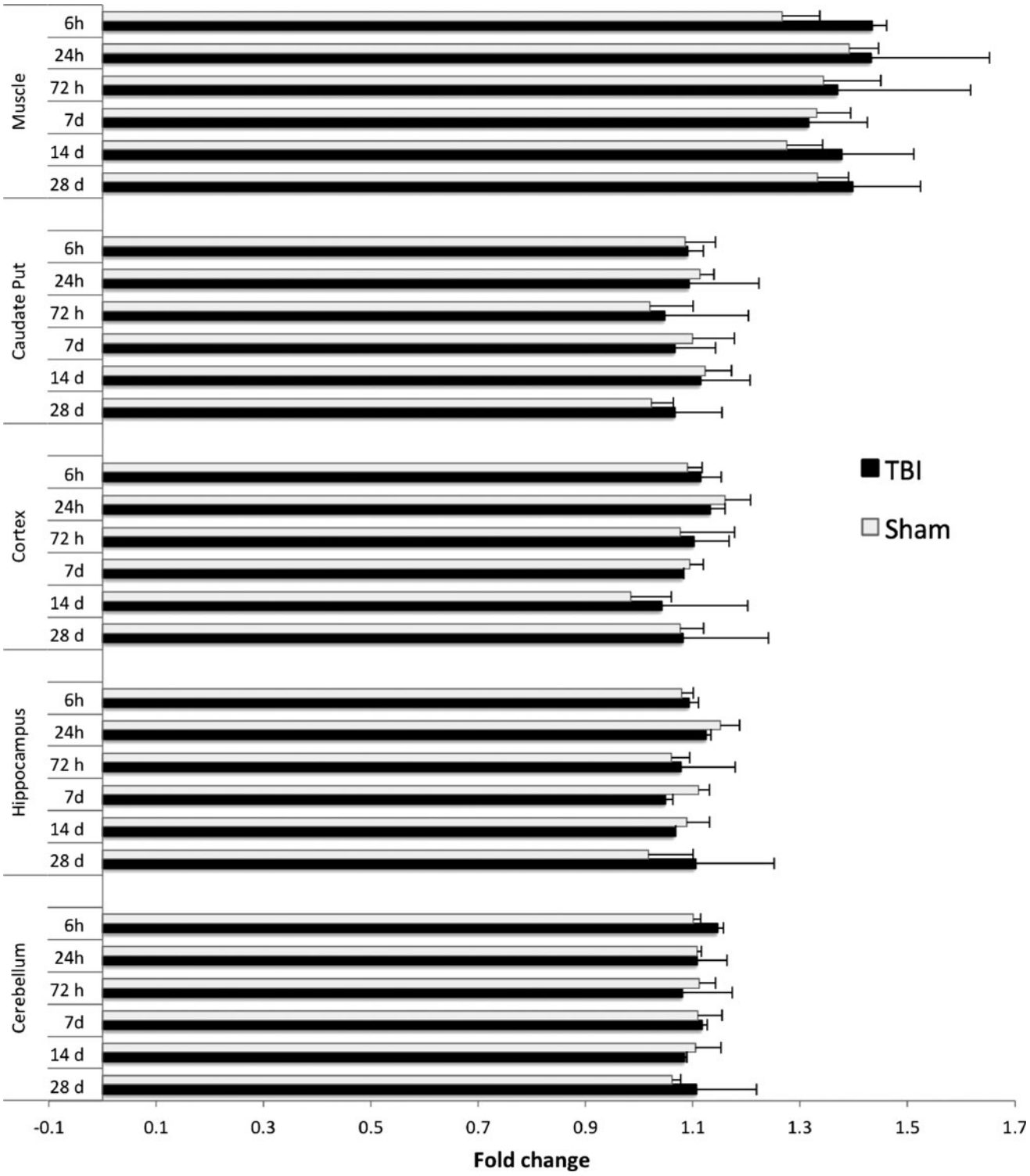

FIG. 5. Mean intensity fold change of Gd-contrast enhanced magnetic resonance imaging (MRI) in selected brain and muscle regions of interest (ROIs) of blast-injured and sham mice.

stiff polycarbonate jacket can prevent or minimize Mn^{2+} contrast increase. As shown in Figure 4, MEMRI contrast values in mice exposed to blast in the presence of torso protection were indistinguishable from those of sham subjects. These results show that shielding of the torso prevents not only neuropathological changes caused by blast,[35] but also the changes in Mn^{2+} uptake by the mouse brain.

Discussion

Our findings establish that the exposure of mice to a 30 psig overpressure shockwave, which corresponds to a mild-to-moderate blast, results in the rapid and enduring increase in uptake of Mn^{2+} by brain structures, compared with sham controls, based on an increase in positive contrast in T1-weighted MRI. This augmentation of

positive contrast progresses from ventricular to periventricular brain sites within the first few hours post-blast and, by 48–72 h, it becomes diffuse; it then slowly returns to baseline within a month after exposure to blast. Importantly, torso protection with a polycarbonate body shield covering chest, abdomen, and limbs prevents the increase of MEMRI signal. Further, a single dose of $MnCl_2$ at 40 mg/kg is sufficient to track the evolution of contrast agent permeability and retention over a month without evidence of Mn^{2+}-associated toxicity in experimental subjects. These findings suggest that MEMRI generates anatomically and temporally predictable patterns of progressive increase of image contrast in subjects exposed to mild-moderate blast TBI and that this signal increase might be prevented by strategies, such as torso shielding, that also ameliorate neuroinflammation[1] and traumatic axonal injury.[35] Thus, MEMRI contrast increase may serve as a relatively simple and reliable marker of acute mild-moderate TBI relevant to blast and blunt injury.[33]

MEMRI signal is significantly different in all ROIs analyzed between injured and sham (control) mice up to 2 weeks after injury. The difference is lost at 1 month post-injury. It is known that Mn^{2+} has a very slow efflux rate from the brain and can remain in mouse tissue between 68 and 168 days after injection.[51] However, the usefulness of MEMRI uptake increase as a biomarker is only apparent in the first couple of weeks after blast injury, at least under the conditions of the present study. Future studies should establish the threshold of detectability of MEMRI signal as a biomarker for blast injury in mice using lower, and thus safer, doses of $MnCl_2$, with different manganese compounds and varying degrees of blast pressure.

The increase in positive contrast observed by MRI after systemic injection of $MnCl_2$ is directly attributable to an increase in the concentration of Mn^{2+} in brain tissue.[52] Doses of $MnCl_2$ administered to rodents have been correlated with concentrations achieved in brain tissue using a variety of techniques such as inductively coupled plasma mass spectrometry,[53,54] graphite furnace atomic absorption spectroscopy,[55] inductively coupled plasma atomic emission spectroscopy,[56] and high resolution autoradiography and gamma counting with $^{54}MnCl_2$.[31,57] Doses and routes of administration of $MnCl_2$ that result in different degrees of brain MRI contrast enhancement also have been established.[37,54,58]

MEMRI is accepted as a valid and useful preclinical imaging approach to study neuroarchitecture, neural tracts (connectivity), and cerebral function *in vivo*.[10,15,17,37,59] The paramagnetic nature of divalent manganese ions (Mn^{2+}), which is administered to animals in the form of the inorganic salt $MnCl_2$, allows it to function as a T1 MRI contrast agent. Mn^{2+} uptake by the central nervous system (CNS) appears to be both a passive process (secondary to the breakdown of the BBB), and an active transfer utilizing specific transporters. Mn^{2+} may compete with Ca^{2+} for passage through several types of voltage-gated Ca^{2+} channels[25,26] and with iron for transport through the divalent metal transporter (DMT-1, DCT-1, ZIP-8, etc.) in neurons and astrocytes.[26–29] In this fashion, Mn^{2+} uptake imitates the physiological uptake of Ca^{2+} and iron and thus becomes a marker of neuronal activity.[15,37,60] Its rapid uptake, slow efflux from the brain, and general tissue retention over time allows for MEMRI to be used to image acute events, such as exposure to drugs, environmental aggressors or, in our case, blast injury. Several studies focusing on MEMRI and other MRI techniques in the diagnosis of TBI have been published, but most have focused on chronic or acute penetrating TBI[61,62] or diffuse blunt trauma.[33] As far as we know, ours is the first study using MEMRI as a biological marker for acute TBI related to blast.

The temporal and anatomical pattern of Mn^{2+} distribution in the brain following blast exposure suggests a compromise of BBB integrity. However, the exploration of BBB permeability with Gd was negative in our study. It is known that in order for the BBB to become permeable to Gd, a significant vascular network breakdown and/or necrosis must be present.[63,64] In fact, small brain tumors and lesions with intact vessels are frequently not detectable with Gd-enhanced MRI. Therefore, in blast TBI, even though a BBB breakdown might be a factor in Mn^{2+} uptake, Gd is unable to detect it and therefore, MEMRI appears to be a more sensitive indicator of BBB integrity than Gd. Active uptake by Ca^{2+}-gated channels is another possible mechanism involved in the incorporation of Mn^{2+} after blast exposure. Several studies have shown disturbance of calcium homeostasis in TBI and promising beneficial effects of calcium channel blockers.[65–68] Future studies should explore the potential effect of calcium channel blockers in reducing MEMRI signal enhancement after TBI.

The increased MEMRI contrast after blast may simply be an exaggeration of the normal process of Mn^{2+} uptake, especially since the temporal–anatomical pattern of uptake is not qualitatively different between blast and sham condition.[31,32] MEMRI contrast enhancement is first apparent at the interventricular foramen and then progresses from the ventricles outwards into the brain parenchyma, thus suggesting that impairments in blood–CNS barriers may play a role; such impairments may be more evident in the blood–cerebrospinal fluid barrier of tela choroidea[69] and in the BBB itself. Other mechanisms may be related to disturbances in calcium homeostasis associated with TBI as mentioned above; a massive influx of Mn^{2+} detected by MEMRI may ''image'' the increased influx of Ca^{2+} occurring in the first few hours after blast exposure.[68,70–72]

Mn^{2+} is a trace element essential for the normal development and function of the brain, but it also has been shown to be neurotoxic particularly in primates and humans.[73,74] Specifically, chronic exposure to high levels of the ion can result in teratogenicity[75–77] and extrapyramidal motor dysfunction, a neurodegenerative disorder that resembles Parkinson's disease.[78–82] Toxicity is partly the result of Mn^{2+} acting as an analog of Ca^{2+} in processes such as synaptic neurotransmission and partly, the result of its role as an oxidant.[83,84] The single dose of $MnCl_2$ administered to mice in the present study does not produce neurological deficits.[85] In fact, mice and rats tolerate well doses of $MnCl_2$ up to 175 mg/kg.[86,87] In agreement with previous reports, mice did not exhibit signs of toxicity such as changes in weight, attitude and activity, appetite, hydration, coat appearance, posture and gait, movement, and complications at the injection site in our study.[58,85] Still, because of evidence that 40 mg/kg of $MnCl_2$ may be mildly neurotoxic,[31,37,88] the use of $MnCl_2$ as a potential diagnostic for TBI must be presently restricted to preclinical studies. However, the enormous potential for Mn^{2+} as a contrast agent in the clinic warrants future research efforts to focus on 1) the development of less toxic manganese-based chelates, clusters, and nanoparticles such as those presently being developed 2) the use of higher magnetic fields and improved imaging sequences that require much lower dosage of Mn^{2+} for detectability by MRI; and 3) the potential co-administration of drugs that protect against the harmful effects of Mn^{2+} such as the anti-oxidant lycopene.[84]

All mice were included in data analysis, irrespective of whether they died or not. We do not attribute the deaths of mice in the course of the study to Mn^{2+} toxicity. Blast injury is known to cause lesions in organs other than the brain.[35] There is a possibility, therefore, that these subjects died for reasons directly related to the blast and not to $MnCl_2$ administration.

In the clinic, CT is the routine first-line imaging modality to assess type and extent of TBI. However, MRI is more sensitive in identifying small structural changes, especially in white matter. MRI techniques employed in the assessment of TBI include conventional MRI for gross anatomical changes—such as contusions and atrophy—or special sequences—such as diffusion weighted imaging to diagnose cerebral edema and ischemia and susceptibility weighted imaging to identify micro-hemorrhages accompanying diffuse axonal injury. However, such approaches have limited value in diagnosing or evaluating mild TBI (concussion). In addition, multi-modal MRI approaches have not yet been implemented in most clinical protocols because standardization is difficult to achieve due to variation in quantitative imaging thresholds, to measurement methodologies, and to fractional anisotropy values in various brain structures at different stages of injury. Therefore, the development of imaging modalities with less variability in important measures remains a high priority, especially for subtle changes associated with mild TBI.

Our findings in this paper indicate that MEMRI signal increase may represent a biomarker for mild-moderate blast TBI. Future studies using blast exposures of lower intensity are pivotal in order to establish the limits/threshold of detectability of MEMRI changes in mild TBI. In addition, comparative studies investigating MEMRI contrast increase between blast and blunt TBI are warranted as the early and accurate detection of mild TBI is not only important for diagnostic and dispositional decisions (e.g., return to play), but also to initiate early treatment and thus improve clinical outcomes.

Acknowledgments

We would like to acknowledge Dr. Ibolja Cernak, University of Alberta, Canada, for the pioneering ideas behind the projects' inception and funding. Blast experiments were performed in the Applied Physics Laboratory at Johns Hopkins University. All imaging experiments were performed in the Georgetown-Lombardi Comprehensive Cancer Center's Preclinical Imaging Research Laboratory, partially supported by the Cancer Center Support Grant P30 CA51008-21. Animal importation into the Preclinical Imaging Research Laboratory was assisted by the Division of Comparative Medicine at Georgetown University Medical Center. Funding provided by: DOD DM102465 (Cernak, PI, Albanese, subcontract PI), NIH P30 CA51008-18 (Weiner) and ABC2 (Albanese); Maryland Stem Cell Research Fund 2011-MSCRF-22-0067-00 (Koliatsos).

Author Disclosure Statement

No competing financial interests exist.

References

1. Cernak, I. and Noble-Haeusslein, L.J. (2010). Traumatic brain injury: an overview of pathobiology with emphasis on military populations. J. Cereb. Blood Flow Metab. 30, 255–266.
2. Warden, D. (2006). Military TBI during the Iraq and Afghanistan wars. J. Head Trauma Rehabil. 21, 398–402.
3. Omalu, B.I., Mancuso, J.A., Cho, P., and Wecht, C.H. (2005). Diagnosis of Alzheimer's disease in an exhumed decomposed brain after twenty months of burial in a deep grave. J. Forensic Sci. 50, 1453–1458.
4. Goldstein, L.E., Fisher, A.M., Tagge, C.A., Zhang, X.L., Velisek, L., Sullivan, J.A., Upreti, C., Kracht, J.M., Ericsson, M., Wojnarowicz, M.W., Goletiani, C.J., Maglakelidze, G.M., Casey, N., Moncaster, J.A., Minaeva, O., Moir, R.D., Nowinski, C.J., Stern, R.A., Cantu, R.C., Geiling, J., Blusztajn, J.K., Wolozin, B.L., Ikezu, T., Stein, T.D., Budson, A.E., Kowall, N.W., Chargin, D., Sharon, A., Saman, S., Hall, G.F., Moss, W.C., Cleveland, R.O., Tanzi, R.E., Stanton, P.K., and McKee, A.C. (2012). Chronic traumatic encephalopathy in blast-exposed military veterans and a blast neurotrauma mouse model. Sci. Transl. Med. 4, 134ra160.
5. Zetterberg, H., Smith, D.H., and Blennow, K. (2013). Biomarkers of mild traumatic brain injury in cerebrospinal fluid and blood. Nat. Rev. Neurol. 9, 201–210.
6. Baldea, J.D. (2014). In response to: time to re-think the Zurich Guidelines? A critique on the consensus statement on concussion in Sport: the 4th International Conference on Concussion in Sport, held in Zurich, November 2012. Clin. J. Sport Med. 24, 521–522.
7. Gioia, G.A. (2015). Multimodal evaluation and management of children with concussion: using our heads and available evidence. Brain Inj. 29, 195–206.
8. McCrory, P., Meeuwisse, W.H., Aubry, M., Cantu, B., Dvorak, J., Echemendia, R.J., Engebretsen, L., Johnston, K., Kutcher, J.S., Raftery, M., Sills, A., Benson, B.W., Davis, G.A., Ellenbogan, R., Guskiewicz, K., Herring, S.A., Iverson, G.L., Jordan, B.D., Kissick, J., McCrea, M., McIntosh, A.S., Maddocks, D., Makdissi, M., Purcell, L., Putukian, M., Schneider, K., Tator, C.H., and Turner, M. (2013). Consensus statement on concussion in sport: the 4th International Conference on Concussion in Sport held in Zurich, November 2012. J. Am. Coll. Surg. 216, e55–e71.
9. Caride, V.J., Sostman, H.D., Winchell, R.J., and Gore, J.C. (1984). Relaxation enhancement using liposomes carrying paramagnetic species. Magn. Reson. Imaging 2, 107–112.
10. Koretsky, A.P. and Silva, A.C. (2004). Manganese-enhanced magnetic resonance imaging (MEMRI). NMR Biomed. 17, 527–531.
11. Lauterbur, P.C. (1989). Image formation by induced local interactions. Examples employing nuclear magnetic resonance. 1973. Clin. Orthopaed. Relat. Res. 3–6.
12. Mendonca-Dias, M.H., Gaggelli, E., and Lauterbur, P.C. (1983). Paramagnetic contrast agents in nuclear magnetic resonance medical imaging. Sem. Nucl. Med. 13, 364–376.
13. Anderson, D.W., Yamanashi, W.S., and Fricke, S.M. (1987). Frequency-dependence of relaxation-times for Mncl2 and Nicl2 Solutions. Med. Phys. 14, 709–709.
14. Anderson, D.W., Yamanashi, W.S., Fricke, S.M., and Lester, P.D. (1987). Frequency-dependence of relaxation properties of aqueous Mncl2 and Nicl2 used for acceptance testing and quality-control of Mr-imagers - 10.7 to 270 Mhz. Invest. Radiol. 22, S9–S9.
15. Lin, Y.J. and Koretsky, A.P. (1997). Manganese ion enhances T1-weighted MRI during brain activation: an approach to direct imaging of brain function. Magn. Reson. Med. 38, 378–388.
16. Newland, M.C., Ceckler, T.L., Kordower, J.H., and Weiss, B. (1989). Visualizing manganese in the primate basal ganglia with magnetic resonance imaging. Exp. Neurol. 106, 251–258.
17. Pautler, R.G., Silva, A.C., and Koretsky, A.P. (1998). In vivo neuronal tract tracing using manganese-enhanced magnetic resonance imaging. Magn. Reson. Med. 40, 740–748.
18. Shirakuni, T., Nagashima, T., Tamaki, N., and Matsumoto, S. (1985). Magnetic resonance imaging of experimental brain edema in cats. Neurosurgery 17, 557–563.
19. Burke, C., Grant, L.A., Goh, V., and Griffin, N. (2013). The role of hepatocyte-specific contrast agents in hepatobiliary magnetic resonance imaging. Semin. Ultrasound CT MR 34, 44–53.
20. Rofsky, N.M. and Earls, J.P. (1996). Mangafodipir trisodium injection (Mn-DPDP). A contrast agent for abdominal MR imaging. Mag. Reson. Imaging Clin. N. Am. 4, 73–85.
21. Schuhmann-Giampieri, G. (1993). Liver contrast media for magnetic resonance imaging. Interrelations between pharmacokinetics and imaging. Invest. Radiol. 28, 753–761.
22. Lyden, A., Larsson, B.S., and Lindquist, N.G. (1983). Autoradiography of manganese: accumulation and retention in the pancreas. Acta Pharmacol. Toxicol. 52, 205–210.
23. Semelka, R.C. and Ascher, S.M. (1993). MR imaging of the pancreas. Radiology 188, 593–602.
24. Steiner, E., Stark, D.D., Hahn, P.F., Saini, S., Simeone, J.F., Mueller, P.R., Wittenberg, J., and Ferrucci, J.T. (1989). Imaging of pancreatic neoplasms: comparison of MR and CT. AJR Am. J. Roentgenol. 152, 487–91.
25. Crossgrove, J.S. and Yokel, R.A. (2005). Manganese distribution across the blood-brain barrier. IV. Evidence for brain influx through store-operated calcium channels. Neurotoxicology 26, 297–307.
26. Tuschl, K., Mills, P.B., and Clayton, P.T. (2013). Manganese and the brain. Int. Rev. Neurobiol. 110, 277–312.

27. Conrad, M.E. and Umbreit, J.N. (2000). Iron absorption and transport—an update. Am. J. Hematol. 64, 287–298.
28. Au, C., Benedetto, A., and Aschner, M. (2008). Manganese transport in eukaryotes: the role of DMT1. Neurotoxicology 29, 569–576.
29. Crossgrove, J.S., Allen, D.D., Bukaveckas, B.L., Rhineheimer, S.S., and Yokel, R.A. (2003). Manganese distribution across the blood-brain barrier. I. Evidence for carrier-mediated influx of managanese citrate as well as manganese and manganese transferrin. Neurotoxicology 24, 3–13.
30. Aschner, M. (1999). Manganese homeostasis in the CNS. Environmental Res. 80, 105–109.
31. Gallez, B., Baudelet, C., and Geurts, M. (1998). Regional distribution of manganese found in the brain after injection of a single dose of manganese-based contrast agents. Magn. Reson. Imaging 16, 1211–1215.
32. London, R.E., Toney, G., Gabel, S.A., and Funk, A. (1989). Magnetic resonance imaging studies of the brains of anesthetized rats treated with manganese chloride. Brain Res. Bull. 23, 229–235.
33. Cernak, I., Vink, R., Zapple, D.N., Cruz, M.I., Ahmed, F., Chang, T., Fricke, S.T., and Faden, A.I. (2004). The pathobiology of moderate diffuse traumatic brain injury as identified using a new experimental model of injury in rats. Neurobiol. Dis. 17, 29–43.
34. Cernak, I. (2010). The importance of systemic response in the pathobiology of blast-induced neurotrauma. Front. Neurol. 1, 151.
35. Koliatsos, V.E., Cernak, I., Xu, L., Song, Y., Savonenko, A., Crain, B.J., Eberhart, C.G., Frangakis, C.E., Melnikova, T., Kim, H., and Lee, D. (2011). A mouse model of blast injury to brain: initial pathological, neuropathological, and behavioral characterization. J. Neuropathol. Exp. Neurol. 70, 399–416.
36. Cernak, I., Merkle, A.C., Koliatsos, V.E., Bilik, J.M., Luong, Q.T., Mahota, T.M., Xu, L., Slack, N., Windle, D., and Ahmed, F.A. (2011). The pathobiology of blast injuries and blast-induced neurotrauma as identified using a new experimental model of injury in mice. Neurobiol. Dis. 41, 538–551.
37. Silva, A.C., Lee, J.H., Aoki, I., and Koretsky, A.P. (2004). Manganese-enhanced magnetic resonance imaging (MEMRI): methodological and practical considerations. NMR Biomed. 17, 532–543.
38. Fricke, S.T., Rodriguez, O., Vanmeter, J., Dettin, L.E., Casimiro, M., Chien, C.D., Newell, T., Johnson, K., Ileva, L., Ojeifo, J., Johnson, M.D., and Albanese, C. (2006). In vivo magnetic resonance volumetric and spectroscopic analysis of mouse prostate cancer models. Prostate 66, 708–717.
39. Pollock, C.B., Rodriguez, O., Martin, P.L., Albanese, C., Li, X., Kopelovich, L., and Glazer, R.I. (2010). Induction of metastatic gastric cancer by peroxisome proliferator-activated receptordelta activation. PPAR Res. 2010, 571783.
40. Rodriguez, O., Fricke, S., Chien, C., Dettin, L., VanMeter, J., Shapiro, E., Dai, H.N., Casimiro, M., Ileva, L., Dagata, J., Johnson, M.D., Lisanti, M.P., Koretsky, A., and Albanese, C. (2006). Contrast-enhanced in vivo imaging of breast and prostate cancer cells by MRI. Cell Cycle 5, 113–119.
41. Sirajuddin, P., Das, S., Ringer, L., Rodriguez, O.C., Sivakumar, A., Lee, Y.C., Uren, A., Fricke, S.T., Rood, B., Ozcan, A., Wang, S.S., Karam, S., Yenugonda, V., Salinas, P., Petricoin, E., 3rd, Pishvaian, M., Lisanti, M.P., Wang, Y., Schlegel, R., Moasser, B., and Albanese, C. (2012). Quantifying the CDK inhibitor VMY-1-103's activity and tissue levels in an in vivo tumor model by LC-MS/MS and by MRI. Cell Cycle 11, 3801–3809.
42. Vissapragada, S., Ghosh, A., Ringer, L., Salinas, P., Brophy, A., Peaceman, D., Kallakury, B., Banerjee, P.P., Fricke, S.T., Helfrich, W., Lee, Y.C., Pestell, R., Scherer, P., Tanowitz, H.B., Avantaggiati, M.L., Hilakivi-Clarke, L., Lisanti, M.P., Rodriguez, O.C., and Albanese, C. (2010). Dietary n-3 polyunsaturated fatty acids fail to reduce prostate tumorigenesis in the PB-ErbB-2×Pten(+/-) preclinical mouse model. Cell Cycle 9, 1824–1829.
43. Beauchamp, E.M., Ringer, L., Bulut, G., Sajwan, K.P., Hall, M.D., Lee, Y.C., Peaceman, D., Ozdemirli, M., Rodriguez, O., Macdonald, T.J., Albanese, C., Toretsky, J.A., and Uren, A. (2011). Arsenic trioxide inhibits human cancer cell growth and tumor development in mice by blocking Hedgehog/GLI pathway. J. Clin. Invest. 121, 148–160.
44. Tian, Y., Wang, S.S., Zhang, Z., Rodriguez, O.C., Petricoin, E. 3rd, Shih, I.M., Chan, D., Avantaggiati, M., Yu, G., Ye, S., Clarke, R., Wang, C., Zhang, B., Wang, Y., and Albanese, C. (2014). Integration of network biology and imaging to study cancer phenotypes and responses. IEEE/ACM Trans. Comput. Biol. Bioinform. 11, 1009–1019.
45. Barzo, P., Marmarou, A., Fatouros, P., Corwin, F., and Dunbar, J. (1996). Magnetic resonance imaging-monitored acute blood-brain barrier changes in experimental traumatic brain injury. J. Neurosurg. 85, 1113–1121.
46. Runge, V.M., Clanton, J.A., Price, A.C., Wehr, C.J., Herzer, W.A., Partain, C.L., and James, A.E. Jr. (1985). The use of Gd DTPA as a perfusion agent and marker of blood-brain barrier disruption. Magn. Reson. Imaging 3, 43–55.
47. Runge, V.M., Schoerner, W., Niendorf, H.P., Laniado, M., Koehler, D., Claussen, C., Felix, R., and James, A.E., Jr. (1985). Initial clinical evaluation of gadolinium DTPA for contrast-enhanced magnetic resonance imaging. Magn. Reson. Imaging 3, 27–35.
48. Norman, A.B., Bertram, K.J., Thomas, S.R., Pratt, R.G., Samaratunga, R.C., and Sanberg, P.R. (1991). Magnetic resonance imaging of rat brain following in vivo disruption of the cerebral vasculature. Brain Res. Bull. 26, 593–597.
49. Waubant, E. (2006). Biomarkers indicative of blood-brain barrier disruption in multiple sclerosis. Dis. Markers 22, 235–244.
50. Essig, M., Weber, M.A., von Tengg-Kobligk, H., Knopp, M.V., Yuh, W.T., and Giesel, F.L. (2006). Contrast-enhanced magnetic resonance imaging of central nervous system tumors: agents, mechanisms, and applications. Topics Magn. Reson. Imaging 17, 89–106.
51. Furchner, J.E., Richmond, C.R., and Drake, G.A. (1966). Comparative metabolism of radionuclides in mammals. 3. Retention of manganese-54 in the mouse, rat, monkey and dog. Health Phys. 12, 1415–1423.
52. Crossgrove, J. and Zheng, W. (2004). Manganese toxicity upon overexposure. NMR Biomed. 17, 544–553.
53. Fa, Z., Zhang, P., Huang, F., Li, P., Zhang, R., Xu, R., Wen, Z., and Jiang, X. (2010). Activity-induced manganese-dependent functional MRI of the rat visual cortex following intranasal manganese chloride administration. Neurosci. Lett. 481, 110–114.
54. Chuang, K.H., Koretsky, A.P., and Sotak, C.H. (2009). Temporal changes in the T1 and T2 relaxation rates (DeltaR1 and DeltaR2) in the rat brain are consistent with the tissue-clearance rates of elemental manganese. Magn. Reson. Med. 61, 1528–1532.
55. Erikson, K.M., John, C.E., Jones, S.R., and Aschner, M. (2005). Manganese accumulation in striatum of mice exposed to toxic doses is dependent upon a functional dopamine transporter. Environmental Toxicol. Pharmacol. 20, 390–394.
56. Ni, Y., Petre, C., Bosmans, H., Miao, Y., Grant, D., Baert, A.L., and Marchal, G. (1997). Comparison of manganese biodistribution and MR contrast enhancement in rats after intravenous injection of MnDPDP and MnCl2. Acta Radiol. 38, 700–707.
57. Gallez, B., Baudelet, C., Adline, J., Geurts, M., and Delzenne, N. (1997). Accumulation of manganese in the brain of mice after intravenous injection of manganese-based contrast agents. Chem. Res. Toxicol. 10, 360–363.
58. Grunecker, B., Kaltwasser, S.F., Peterse, Y., Samann, P.G., Schmidt, M.V., Wotjak, C.T., and Czisch, M. (2010). Fractionated manganese injections: effects on MRI contrast enhancement and physiological measures in C57BL/6 mice. NMR Biomed. 23, 913–921.
59. Inoue, T., Majid, T., and Pautler, R.G. (2011). Manganese enhanced MRI (MEMRI): neurophysiological applications. Rev. Neurosci. 22, 675–694.
60. Van der Linden, A., Verhoye, M., Van Meir, V., Tindemans, I., Eens, M., Absil, P., and Balthazart, J. (2002). In vivo manganese-enhanced magnetic resonance imaging reveals connections and functional properties of the songbird vocal control system. Neuroscience 112, 467–474.
61. Bouilleret, V., Cardamone, L., Liu, Y.R., Fang, K., Myers, D.E., and O'Brien, T.J. (2009). Progressive brain changes on serial manganese-enhanced MRI following traumatic brain injury in the rat. J. Neurotrauma 26, 1999–2013.
62. Watts, L.T., Shen, Q., Deng, S., Chemello, J., and Duong, T.Q. (2014). Manganese-enhanced MRI of traumatic brain injury. J. Neurotrauma.
63. Young, G.S. (2007). Advanced MRI of adult brain tumors. Neurol. Clin. 25, 947–973.
64. Blanchette, M., Tremblay, L., Lepage, M., and Fortin, D. (2014). Impact of drug size on brain tumor and brain parenchyma delivery after a blood-brain barrier disruption. J. Cereb. Blood Flow Metab. 34, 820–826.
65. Geyer, C., Ulrich, A., Grafe, G., Stach, B., and Till, H. (2009). Diagnostic value of S100B and neuron-specific enolase in mild pediatric traumatic brain injury. J. Neurosurg. Pediatrics 4, 339–344.
66. Maneshi, M.M., Sachs, F., and Hua, S.Z. (2015). A threshold shear force for calcium influx in an astrocyte model of traumatic brain injury. J. Neurotrauma 32, 1020–1029.

67. Shahlaie, K., Gurkoff, G.G., Lyeth, B.G., Muizelaar, J.P., and Berman, R.F. (2013). Neuroprotective effects of SNX-185 in an in vitro model of TBI with a second insult. Restor. Neurol. Neurosci. 31, 141–153.
68. Weber, J.T. (2012). Altered calcium signaling following traumatic brain injury. Front. Pharmacol. 3, 60.
69. Damkier, H.H., Brown, P.D., and Praetorius, J. (2013). Cerebrospinal fluid secretion by the choroid plexus. Physiol. Rev. 93, 1847–1892.
70. Gurkoff, G., Shahlaie, K., Lyeth, B., and Berman, R. (2013). Voltage-gated calcium channel antagonists and traumatic brain injury. Pharmaceuticals 6, 788–812.
71. Geddes-Klein, D.M., Serbest, G., Mesfin, M.N., Cohen, A.S., and Meaney, D.F. (2006). Pharmacologically induced calcium oscillations protect neurons from increases in cytosolic calcium after trauma. J. Neurochem. 97, 462–474.
72. Spaethling, J.M., Klein, D.M., Singh, P., and Meaney, D.F. (2008). Calcium-permeable AMPA receptors appear in cortical neurons after traumatic mechanical injury and contribute to neuronal fate. J. Neurotrauma 25, 1207–1216.
73. Dobson, A.W., Erikson, K.M., and Aschner, M. (2004). Manganese neurotoxicity. Ann. N. Y. Acad. Sci. 1012, 115–128.
74. Racette, B.A., Antenor, J.A., McGee-Minnich, L., Moerlein, S.M., Videen, T.O., Kotagal, V., and Perlmutter, J.S. (2005). [18F]FDOPA PET and clinical features in parkinsonism due to manganism. Movement Disord. 20, 492–496.
75. Arias, E. and Zavanella, T. (1979). Teratogenic effects of manganese ethylenebisdithiocarbamate (MANEB) on forelimb regeneration in the adult newt, Triturus cristatus carnifex. Bulletin of environmental contamination and toxicology 22, 297–304.
76. Deskin, R., Bursian, S.J., and Edens, F.W. (1981). Neurochemical alterations induced by manganese chloride in neonatal rats. Neurotoxicology 2, 65–73.
77. Zhen, Z. and Xie, J. (2012). Development of manganese-based nanoparticles as contrast probes for magnetic resonance imaging. Theranostics 2, 45–54.
78. Autissier, N., Rochette, L., Dumas, P., Beley, A., Loireau, A., and Bralet, J. (1982). Dopamine and norepinephrine turnover in various regions of the rat brain after chronic manganese chloride administration. Toxicology 24, 175–182.
79. Barbeau, A. (1984). Manganese and extrapyramidal disorders (a critical review and tribute to Dr. George C. Cotzias). Neurotoxicology 5, 13–35.
80. Calne, D.B., Chu, N.S., Huang, C.C., Lu, C.S., and Olanow, W. (1994). Manganism and idiopathic parkinsonism: similarities and differences. Neurology 44, 1583–1586.
81. Huang, C.C., Lu, C.S., Chu, N.S., Hochberg, F., Lilienfeld, D., Olanow, W., and Calne, D.B. (1993). Progression after chronic manganese exposure. Neurology 43, 1479–1483.
82. Kilburn, C.J. (1987). Manganese, malformations and motor disorders: findings in a manganese-exposed population. Neurotoxicology 8, 421–429.
83. Milatovic, D., Zaja-Milatovic, S., Gupta, R.C., Yu, Y., and Aschner, M. (2009). Oxidative damage and neurodegeneration in manganese-induced neurotoxicity. Toxicol. Appl. Pharmacol. 240, 219–225.
84. Lebda, M.A., El-Neweshy, M.S., and El-Sayed, Y.S. (2012). Neurohepatic toxicity of subacute manganese chloride exposure and potential chemoprotective effects of lycopene. Neurotoxicology 33, 98–104.
85. Bock, N.A., Paiva, F.F., and Silva, A.C. (2008). Fractionated manganese-enhanced MRI. NMR Biomed. 21, 473–478.
86. Aoki, I., Wu, Y.J., Silva, A.C., Lynch, R.M., and Koretsky, A.P. (2004). In vivo detection of neuroarchitecture in the rodent brain using manganese-enhanced MRI. NeuroImage 22, 1046–1059.
87. Lee, J.H., Silva, A.C., Merkle, H., and Koretsky, A.P. (2005). Manganese-enhanced magnetic resonance imaging of mouse brain after systemic administration of MnCl2: dose-dependent and temporal evolution of T1 contrast. Magn. Reson. Med. 53, 640–648.
88. Dodd, C.A., Ward, D.L., and Klein, B.G. (2005). Basal Ganglia accumulation and motor assessment following manganese chloride exposure in the C57BL/6 mouse. Int. J. Toxicol. 24, 389–397.

Address correspondence to:
Olga Rodriguez, PhD, MD
Department of Oncology
Lombardi Comprehensive Cancer Center
Georgetown University Medical Center
3970 Reservoir Road NW
The Research Building, Room WB01
Washington, DC 20057

E-mail: rodriguo@georgetown.edu